NeuroImage 231 (2021) 117866

Contents lists available at ScienceDirect

NeuroImage

journal homepage: www.elsevier.com/locate/neuroimage

Neural generators of the frequency-following response elicited to stimuli of low and high frequency: A magnetoencephalographic (MEG) study

Natàlia Gorina-Careta[a,b,c], Jari L.O. Kurkela[d], Jarmo Hämäläinen[d], Piia Astikainen[d], Carles Escera[a,b,c,*]

[a] Brainlab-Cognitive Neuroscience Research Group, Department of Clinical Psychology and Psychobiology, University of Barcelona, P. Vall d'Hebron 171, Barcelona 08035, Catalonia-Spain
[b] Institute of Neurosciences, University of Barcelona, P. Vall d'Hebron 171, Barcelona 08035, Catalonia-Spain
[c] Institut de Recerca Sant Joan de Déu (IRSJD), Santa Rosa 39-57, Esplugues de Llobregat, Catalonia, Barcelona 08950, Spain
[d] Centre for Interdisciplinary Brain Research, Department of Psychology, Faculty of Education and Psychology, University of Jyvaskyla, Jyväskylä, Finland

ARTICLE INFO

Keywords:
Frequency following responses
Magnetoencephalography
Neural sources
Auditory plasticity
Speech sound encoding
Fundamental frequency

ABSTRACT

The frequency-following response (FFR) to periodic complex sounds has gained recent interest in auditory cognitive neuroscience as it captures with great fidelity the tracking accuracy of the periodic sound features in the ascending auditory system. Seminal studies suggested the FFR as a correlate of subcortical sound encoding, yet recent studies aiming to locate its sources challenged this assumption, demonstrating that FFR receives some contribution from the auditory cortex. Based on frequency-specific phase-locking capabilities along the auditory hierarchy, we hypothesized that FFRs to higher frequencies would receive less cortical contribution than those to lower frequencies, hence supporting a major subcortical involvement for these high frequency sounds. Here, we used a magnetoencephalographic (MEG) approach to trace the neural sources of the FFR elicited in healthy adults ($N = 19$) to low (89 Hz) and high (333 Hz) frequency sounds. FFRs elicited to the high and low frequency sounds were clearly observable on MEG and comparable to those obtained in simultaneous electroencephalographic recordings. Distributed source modeling analyses revealed midbrain, thalamic, and cortical contributions to FFR, arranged in frequency-specific configurations. Our results showed that the main contribution to the high-frequency sound FFR originated in the inferior colliculus and the medial geniculate body of the thalamus, with no significant cortical contribution. In contrast, the low-frequency sound FFR had a major contribution located in the auditory cortices, and also received contributions originating in the midbrain and thalamic structures. These findings support the multiple generator hypothesis of the FFR and are relevant for our understanding of the neural encoding of sounds along the auditory hierarchy, suggesting a hierarchical organization of periodicity encoding.

1. Introduction

The frequency-following response (FFR; Moushegian et al., 1973) has gained recent interest in auditory cognitive neuroscience as it captures with great fidelity the tracking accuracy of the periodic sound features in the ascending auditory system. In particular, it reflects synchronous and sustained neural phase-locking to the spectral and temporal periodic characteristics of the eliciting acoustic signal in the range of approximately 100 to 1500 Hz (Galbraith et al., 2000; Picton, 2011), thus faithfully mimicking the eliciting stimulus as it unfolds in time.

The FFR can be recorded from the scalp with both electroencephalography (EEG) and magnetoencephalography (MEG) and it emerges at circa 7–15 ms from sound onset. By means of a range of analytical tools in the temporal and spectral domains, it provides an objective insight into the neural encoding of the acoustic features intrinsic to speech sounds, including timing (onsets and offsets), pitch (fundamental frequency: f0) and temporal fine structure (harmonics information) (Kraus et al., 2017; Krizman and Kraus, 2019; Ribas-Prats et al., 2019; Skoe and Kraus, 2010a). By decomposing the FFR in the temporal and spectral domains, it is possible to obtain a snapshot of how sounds are transcribed and encoded throughout the auditory hierarchy, and how these neural sound traces are shaped by context, experience and challenging conditions. Indeed, the FFR is highly sensitive to context-dependent contingencies (Chandrasekaran et al., 2014; Gorina-Careta et al., 2016; Skoe et al., 2014; Slabu et al., 2012) and to real-time statistical properties of a particular stimulus (Chandrasekaran et al.,

* Corresponding author.
E-mail address: cescera@ub.edu (C. Escera).

https://doi.org/10.1016/j.neuroimage.2021.117866
Received 7 July 2020; Received in revised form 8 February 2021; Accepted 9 February 2021
Available online 13 February 2021

2009; Escera, 2017; Skoe et al., 2015, 2013; Skoe and Kraus, 2010b), and it provides a non-invasive measure of how short-term auditory training (Russo et al., 2005; Song et al., 2008, 2012; Carcagno and Plack, 2011; for review see Carcagno and Plack, 2017) and auditory experiences, such as with language (Krishnan et al., 2008; Krizman et al., 2015, 2014, 2012; Skoe et al., 2017) and musical training (Bidelman et al., 2011; Musacchia et al., 2007; Parbery-Clark et al., 2011, 2009; Skoe and Kraus, 2012; Wong et al., 2007), shape sound representation in a subcortico-cortical auditory network (Kraus and Slater, 2016; Kraus and White-Schwoch, 2015). Moreover, the FFR has become a valuable tool to evaluate the neural encoding of sounds in challenging conditions, such as listening in noise (Li and Jeng, 2011; Russo et al., 2004), and changes in encoding due to aging (Anderson, 2017) and learning, as well as abnormalities related to speech and language disorders (Anderson et al., 2010; Banai et al., 2009, 2005; Banai and Ahissar, 2006; Chandrasekaran et al., 2009; Cunningham et al., 2001; Hornickel et al., 2012; Hornickel and Kraus, 2013; Russo et al., 2009, 2008).

Notably, despite the accumulation of studies on the FFR, no clear picture has emerged so far regarding its anatomical generators, and certain controversy is still being debated. A conventional view from early seminal studies stated that the FFR has a central, rather than a cochlear origin, and that its generators can be attributed solely to neuronal aggregates in caudal brainstem and midbrain structures, with the inferior colliculus (IC) being the major neuronal source. This midbrain origin is supported by the fact that the short-latency of the FFR aligns with the latency of the first spikes in IC in the cat (Langner and Schreiner, 1988) and since human FFRs contain phase-locked activity up to 1500 Hz, which spans beyond the upper limit of phase-locking capabilities of cortical neurons (~100 Hz; Aiken and Picton, 2008). Additional evidence comes from comparisons between deep and scalp recordings in animal models (Smith et al., 1975) as well as from animal lesion studies, where it was observed that an electrocoagulated lesion and the cryogenic cooling of the IC result in the abolishment of FFRs, with subsequent heating in this later case yielding a recovery of the responses both in the IC and at the scalp (Kiren et al., 1994; Marsh et al., 1970; Smith et al., 1975). Human studies in patients with brain injuries (Sohmer et al., 1977; White-Schwoch et al., 2019) and source reconstruction studies (Bidelman, 2015; Zhang and Gong, 2017) also support this view, thus providing evidence of the FFR being a correlate of subcortical sound encoding. Nevertheless, a mixture of subcortical sources has been recognized in the generation of the FFR (Chandrasekaran and Kraus, 2010; Tichko and Skoe, 2017) and other subcortical contributors were supported by other animal studies that reported weaker contributions of the IC to the FFR, with the major source located in the CN (Gardi et al., 1979) or in the MGB (Weinberger et al., 1970).

Recently, the controversy around the neural origins of the FFR was renewed, with another view proposing the FFR as a representation of the sustained activity from the whole auditory system. Indeed, recent MEG evidence demonstrated that the responses to a complex auditory stimulus of a fundamental frequency close to 100 Hz receive contributions not only from the subcortical nuclei (i.e., the cochlear nucleus and the IC), but also from the medial geniculate body of the thalamus and to a major extent from the auditory cortex (Coffey et al., 2017, 2016; Hartmann and Weisz, 2019), proposing that the FFR recorded from the scalp is an aggregate response with both subcortical and cortical contributions.

The implications of these findings need, however, a re-examination in the light of the phase-locking capabilities of neuronal aggregates along the auditory hierarchy. Indeed, the upper limit of temporal precision in phase-locked firing reduces with each ascending step in the auditory pathway, so that the ability of neurons to follow fast modulations reduces upstream the auditory hierarchy (Batra et al., 1989; Joris et al., 2004; Langner, 1992), and therefore the specific frequency of the eliciting stimulus used to obtain the FFR may play a critical role in engaging multiple sources and a specific configuration of subcortical and cortical generators. Hence, capitalizing on the frequency-specific phase-locking capabilities along the auditory hierarchy, it has been observed that the relative contribution of subcortical and cortical sources to the scalp- recorded FFR, or FFR source configuration, varies systematically with stimulus frequency. In fact, according to a theoretical latency modeling using six generators located along the auditory hierarchy, the cortical contributions to the scalp-recorded EEG-FFR observed were restricted to the lowest (fundamental) frequencies of the speech spectrum (100 Hz), where the cortical component of the FFR was the largest (Tichko and Skoe, 2017). Recent evidence showed that the cortical contribution to the FFR at frequencies higher than 150 Hz is not present (Bidelman, 2018). Interestingly, the seminal studies which ascribed the neural origins of the FFR to exclusively subcortical sources used relatively high-frequency stimuli (> 200 Hz, Langner and Schreiner, 1988; Marsh et al., 1970; Smith et al., 1975; Sohmer et al., 1977), which according to the recent studies (Bidelman, 2018; Tichko and Skoe, 2017), would engage only the subcortical structures of the auditory pathway. This modulation of the FFR source configuration depending on the stimulus frequency is also present when the stimulus frequency is theoretically high enough to reflect neural activity coming exclusively from subcortical structures (Zhang and Gong, 2019), thus providing a hypothesis on the reason why different seminal studies pointed to different subcortical nuclei as the main generators of the FFR. Overall, these recent findings support an emerging viewpoint that the FFR represents an aggregation of phase-locked neural activity from multiple generators along the auditory system, with its specific neural origins depending on the frequency of the eliciting stimulus.

Yet, most of the recent studies regarding the FFR origins have been carried out with EEG, which although having an excellent temporal resolution lacks precise spatial accuracy. Signals recorded in the scalp electrodes are the result of overlapping neural generators from different anatomical structures, which do not allow inferences about the underlying neuroanatomy, and the source reconstruction techniques available in EEG have some limitations (Jackson and Bolger, 2014). On the other hand, MEG has a more accurate spatial resolution due to the properties of the magnetic field and its weak interaction with biologic tissues at the frequencies of brain electric currents, makes it less subject to distortion providing a better localization of sources specially when co-registered with magnetic resonance images (Baillet, 2017; Gross et al., 2013). Therefore, in the present study we used MEG to determine the anatomical contributions to the FFRs elicited to sounds of two different frequencies, low (89 Hz) and high (333 Hz), and to dissociate a hierarchy of anatomical sources contributing to its generation, thus dissociating the contribution of different neural generators to the aggregate FFR measured from the scalp. Considering the previous literature, we hypothesized that FFRs elicited to the high frequency would receive less cortical contribution than those to the low frequency, hence supporting the recent evidence of a frequency-dependent FFR source configuration and the involvement of only subcortical auditory generators in the FFR elicited to high-frequency stimulation.

2. Methods

2.1. Participants

Twenty-three young adults (aged 21–34 years, mean age = 25.3 years, 4 males, 1 left–handed) with no history of auditory, neurological or psychiatric disorders participated in the study. Two participants had to be excluded as they could not finish the anatomical magnetic resonance imaging recording, and two other participants due to excessive eye, neck and mouth movements during the MEG recording, resulting in a final sample of nineteen participants. Hearing thresholds were assessed in each ear with a standard pure-tone audiometry using three test frequencies (250, 500 and 1000 Hz) at the beginning of the experimental session by means of a SA-51 portable screening audiometer (MEDIROLL Medico Technical Ltd, Debrecen, Hungary). The minimum threshold re-

quested for participation was below 25 dB SPL for all tested frequencies and an interaural difference of < 10 dB. As music experience is known to modulate the encoding of the fundamental frequency (F0) of periodic sounds in the subcortical auditory pathway (Song et al., 2011), all participants enrolled had less than four years of musical training that ceased two or more years before the study.

The study was approved by the Bioethical Committee of the University of Barcelona and the Ethics Committee of the University of Jyväskylä and was carried out in accordance with the Code of Ethics of the World Medical Association (Declaration of Helsinki). Written and signed informed consent was obtained from each participant before starting the experiment. Pre-processed MEG and EEG data will be available on request to the corresponding author. All custom-written code used is also available upon request to the corresponding author.

2.2. Stimuli and procedure

The auditory stimuli consisted of two pure sinusoidal tones of 200 ms duration, including 5 ms rise and fall times, with a frequency of 89 and 333 Hz respectively. The stimuli were delivered binaurally at an intensity of ~75 dB in alternating polarities through KAR ADU 1c audio stimulator (KAR-Audio, Unides Design Ay, Helsinki, Finland) with foam insert EAR-tips. The stimuli were generated and presented with Matlab v.2016a (Matworks). The auditory stimulation consisted of two conditions in which each of the stimuli were delivered in a repetitive sequence with a variable SOA ranging between 241 and 265 ms (mean SOA 253 ms) jittered randomly. Each condition was divided in 16 blocks, each containing 950 stimuli (475 stimuli delivered in each polarity), so that the stimuli of each frequency was presented a total of 15,200 times. All the blocks corresponding to each frequency were delivered sequentially, with the order of the conditions counterbalanced across participants. Empty room activity was recorded for a 2-min epoch before each experimental session to estimate the intrinsic noise levels. During the EEG/MEG experiment, participants sat in an electrically, magnetically and acoustically shielded room, with their head accommodated inside the helmet-shaped device, and were instructed to relax and watch a silent movie whilst ignoring the auditory stimulation. Pauses between blocks lasted 30 s to allow the participants to rest, and there was a thirty-minute break between conditions were participants were allowed to move. As the synchronization between the auditory stimulation and the triggers is highly critical in FFR recordings, trigger-stimulus synchronization tests were carried out three times during the experimental period (before starting, after participant #10, and at the end). Results revealed a consistent and stable 12 ms delay for all the triggers in all the three measurements.

2.3. Data acquisition

Simultaneous magnetoencephalogrcaphic and electroencephalographic data were recorded with a 306-channel whole–head system (Elekta Neuromag® TRIUX™, Elekta Oy, Helsinki, Finland) consisting of 204 planar gradiometers and 102 magnetometers, and a compatible 64-channel EEG cap (EASYCAP GmbH, Herrsching, Germany). The EOG was measured with two bipolar electrodes placed above and below the right eye (vertical EOG), and two horizontal electrodes placed on the outer canthi of the eyes (horizontal EOG) and the ground electrode was located in the right collarbone. For the EEG recording, the right earlobe served as an online reference. Five Head Position Indicator coils (HPI-coils) were attached on top of the EEG cap; two on the forehead, two behind the ears and one on the vertex of the head. The locations of three anatomical landmarks (the nasion and left and right preauricular points) and the five HPI-coils, as well as all the locations of all the EEG electrodes and a number of additional points on the head were digitized with an Isotrak 3D digitizer (PolhemusTM, United States) before the experiment started for co-registration with the participant's anatomical MRI. After the thirty-minute break between conditions, the location of five HPI-coils was re-digitized to recalculate the position of the head inside the MEG.

The MEG was recorded in 68° upright gantry position. All EEG impedances were kept below 10 kΩ during the whole recording session and both MEG and EEG data were online bandpass-filtered from 0.1 to 1660 Hz and digitized with a sampling rate of 5 kHz. To ensure that the participant's head position relative to the recording instrument was constant throughout the experiment, the magnetic fields produced by the HPI coils were measured before each block.

Individual structural magnetic resonance images (sMRI) were acquired from a private company offering MRI services (Synlab Jyväskylä, Jyväskylä, Finland). T1-weighted 3D images were collected on a GE 1.5 T (GoldSeal Signa HDxt) MRI scanner using a standard head coil and with the following parameters: repetition time/echo time [TR/TE] = 540/10 ms, flip angle [FA] = 90°, matrix size = 256 × 256, slice thickness = 1.2 mm, sagittal orientation.

2.4. MEG and EEG preprocessing

Continuous MEG data was pre-preprocessed off-line with the Elekta Neuromag™ MaxFilter 2.1 (Elekta Oy, Helsinki, Finland) Signal Space Separation (SSS) method (Taulu et al., 2004) to suppress external magnetic interference and remove and interpolate static bad channels. MaxFilter software was also applied for head movement correction and transforming the head origin to the same position for each participant. MEG data was then imported to Brainstorm (Tadel et al., 2011) for further processing. Eye blink and heart beat artefacts were removed using Brainstorm's source signal projection (SSP) algorithm (Hämäläinen, 2009; Tesche et al., 1995) when the topography of the components matched those of ocular or cardiac origin upon visual inspection. The clean MEG and EEG recordings were filtered with a bandpass Kaiser FIR filter from 75 to 1500 Hz (Filter order = 1612, Stopband attenuation = 60 dB, Passband ripple = 0,1%) and epoched from −40 to 240 ms relative to stimulus onset. Epochs were baseline corrected to a 40 ms interval preceding the sound onset and averaged separately for each frequency condition, polarity of presentation and for each participant separately. Responses to alternating polarity stimuli were subtracted to maximize the response to pure tones (Aiken and Picton, 2008).

2.5. Region of interest analysis from distributed source modeling

The source modeling approach for the present study was based on the methods implemented by Coffey et al. (2016) using for the source analysis of the MEG data obtained from both the gradiometers and the magnetometers. In particular, for the present experiment, the signal source was estimated using distributed source models, which estimate the amplitude of a large number of dipoles distributed throughout the brain volume, but must be constrained by spatial priors (Gross et al., 2013; Hämäläinen et al., 2010; Jensen and Hesse, 2010).

FreeSurfer (Fischl, 2012) was used to prepare the cortical surfaces and automatically segment subcortical structures from each participant's T1-weighted anatomical MRI scan. Anatomical data was later imported to Brainstorm, where precise co-registration of MEG and structural MRI data was accomplished using a semiautomatic procedure. The information of the fiducial points was used for a first alignment and the digitized head shape and the scalp surface of each individual were then used to reduce the minimum distance error between them in an iterative process. Thalamic and brainstem structures were then combined with the cortex surface to form a mixed surface/volume model with the deep brain activity (DBA) model, which included a triangulation of the cortical surface (~15,000 vertices), and brainstem and thalamus as a three-dimensional dipole grid (~18,000 points) (Attal and Schwartz, 2013). The head model was computed using the overlapping – spheres algorithm for each participant. This forward model explains how neural electric currents of the source space produce magnetic fields at the external sensors with good accuracy (Huang et al., 1999). A noise covari-

ance matrix, which accounts for the contaminants that remain present in the data after the preprocessing is complete, was computed from the 2-min empty-room recordings. The inverse solution was calculated on the subtracted polarities average for each participant and frequency condition using wMNE source distribution algorithm (Hämäläinen, 2009; Lin et al., 2006) with unconstrained source orientations using Brainstorm default parameters.

To disentangle the neural contributors of the FFR and isolate the signals originated in specific brain regions, bilateral regions of interest (ROIs) were defined in the main subcortical nuclei and cortical areas that conform the human auditory pathway (i.e., cochlear nucleus, CN; inferior colliculus, IC; medial geniculate body of the thalamus, MGB; and primary auditory cortex, AC), as well as in two control regions that are at the maximal distance from the target auditory regions: the frontal (FP) and occipital (OP) poles. As the head model used was a mixed surface/volume model, the ROIs were defined either as surfaces or volume depending on their location. For the surface ROIs, the right and left AC were defined as the merged regions identified in the Destrieux Atlas (Destrieux et al., 2010) as the transverse temporal gyrus and transverse temporal sulcus (L: 7.07 cm^2 [s.d. = 1.22]; R: 5.41 cm^2 [s.d. = 0.99]). The frontal poles (L: 8.45 cm^2 [s.d. = 1.50]; R: 12.44 cm^2 [s.d. = 2.50]) and the occipital poles (L: 16.76 cm^2 [s.d. = 2.02]; R: 24.86 cm^2 [s.d. = 3.97]) were also defined as surface ROIs. Additionally, spherical subcortical volume ROIs were grown from seeds located in the dipole grid around previously published standardized MNI coordinates (Hofmeier et al., 2018; Mühlau et al., 2006) corresponding to the left and right CN (MNI: [±10, −34, −45]; L: 0.49 cm^2 [s.d. = 0.02]; R: 0.50 cm^2 [s.d. = 0.02]) and left and right IC (MNI: [±6, −33, −11]; L: 0.48 cm^2 [s.d. = 0.02]; R: 0.48 cm^2 [s.d. = 0.03]). Additionally, ROIs capturing the activity from the thalamic MGB were defined based on the standardized MNI ([±17, −24, −2]) and covered approximately the posterior third of the thalamus (L: 1.30 cm^2 [s.d. = 0.02]; R: 1.27 cm^2 [s.d. = 0.03]).

A time series of mean amplitudes was extracted for each ROI and for each of the three orientations in the unconstrained orientation source model for the FFR (30 to 210 ms from stimulus onset) and the baseline (−40 to 0 ms from stimulus onset) periods. To obtain the power spectral profile of the different extracted time series, Fast Fourier Transform (FFT; Cooley and Tukey, 1964) was applied to zero-padded (1-Hz resolution) averages, windowed with a 5-ms raised cosine ramp. However, this approach might rise some concern as the noise floor estimation from the baseline period is much shorter than the FFR segment. A more stringent analysis was applied in which to obtain the power spectral profile of the different time series of the FFR period, FFT was applied to zero-padded (1-Hz resolution) averages, windowed with a 5-ms raised cosine ramp in 40 ms windows with a 50% overlap. The spectral decomposition was then averaged across the 8 resulting windows to obtain one single spectrum for the FFR period. In both FFT analyses, orientations were summed in the frequency domain to obtain a single spectrum for each ROI, and averaged to yield a final single spectrum for each bilateral pair of ROIs during the FFR and the baseline period.

The mean normalized power in each ROI was computed using a 5-Hz-wide window surrounding the f0 of the presented stimuli for both the FFR and the baseline spectra, so that we calculated the increase of signal during FFR at f0 over baseline for each bilateral pair of ROIs and control regions. We then compared this increase in each auditory ROI to the average of the same measure in the control regions. Overall auditory-to-control ratio effects were assessed by means of a repeated-measures ANOVA with the factors Frequency (Low vs. High) and ROI (CN, IC, MGB and PAC). To further analyze the contribution of the different auditory ROIs to the aggregate FFR recorded from the scalp, we assessed statistical significance for each auditory ROI versus control ROIs using Wilcoxon-matched pair tests. The Greenhouse–Geisser correction was applied when the assumption of sphericity was violated, and results were corrected using the Bonferroni correction to adjust for multiple comparisons, so that significance was defined for $p \leq 0.0125$ (0.05/4).

2.6. Comparison of the forward projection of the auditory ROIs

In order to further ascertain the contribution of the different neural generators to the scalp recorded FFR for the two frequencies, we compared the topography of the scalp recorded FFR in both frequencies separately with the topography of the simulated activity from the different auditory ROIs. MEG topographies were obtained by transforming the time domain averages for each frequency and each participant separately to the spectral domain using FFT applied to demeaned, zero-padded (1-Hz resolution) averages within the 30 to 210 ms time-period. Spectral amplitude responses for each sensor were computed by taking the signal at the f0 spectral peak and plotted in a scalp topography, thus providing simulated sensor topographical distributions for each auditory generator source and frequency separately. Similarly, to observe the topography of activity from each paired auditory ROI in the sensor space, we applied the MEG forward model to project the source magnitudes back to the sensor space and obtain simulated time-domain reconstructions as if only the selected ROI was actively contributing to the signal. The simulated time-domain recordings were averaged across participants for each frequency separately and transformed to the spectral domain using a Fast Fourier Transform (FFT) applied to demeaned, zero-padded (1-Hz resolution) averages within the 30 to 210 ms time-period. Spectral amplitude responses for each sensor were computed by taking the signal at the f0 spectral peak and plotted for each sensor in a scalp topography, thus providing simulated sensor topographical distributions for each auditory generator source and frequency separately.

To compare the topographies of the recorded FFR data to the simulated topographies for the four auditory generators for each frequency, we computed a topographical measure of global dissimilarity (Dissimilarity Index) (Costa-Faidella et al., 2011; Murray et al., 2008). The Dissimilarity Index is an index of configuration differences independent of their strength, and provides a statistical means of determining whether the brain networks activated by two conditions differ. The Dissimilarity Index equals the square root of the mean of the squared differences between the signals measured at each sensor, each of which is first scaled to unitary strength by dividing by the instantaneous global field power (the root mean square across the average-referenced sensor values at a given instant in time). The Dissimilarity Index can range from 0 (topographic homogeneity) to 2 (topographic inversion).

2.7. Hemispheric asymmetries of the cortical FFR

We tested for hemispheric differences in cortical FFR sources by performing a two-tailed Wilcoxon signed-rank test on the difference between f0 amplitude during the FFR period (30 to 210 ms) in the right versus left AC ROIs for each individual and for each frequency condition, using the data from the mixed model reported previously. Subcortical ROIs were not tested as they are small areas that are too close together for the model to be accurate enough to separate right and left activity.

3. Results

The grand–average waveforms of FFRs recorded with EEG and MEG and elicited to both frequency conditions are depicted in Fig. 1, together with the corresponding spectral decompositions. FFRs can be observed both in the time and spectral domains for both frequency conditions and using the two recording methods (EEG and MEG; Fig. 1). In the time domain, although the FFRs were visible for both frequency conditions, the FFRs elicited to the low frequency condition had a much larger amplitude compared to those elicited to the high frequency condition. In addition, both MEG recordings had a noisier baseline compared to the EEG ones, but yet it was similar across stimulus frequencies, indicating that the observed noise in the MEG signals can be attributed to the recording technique itself. In the frequency domain, both EEG and

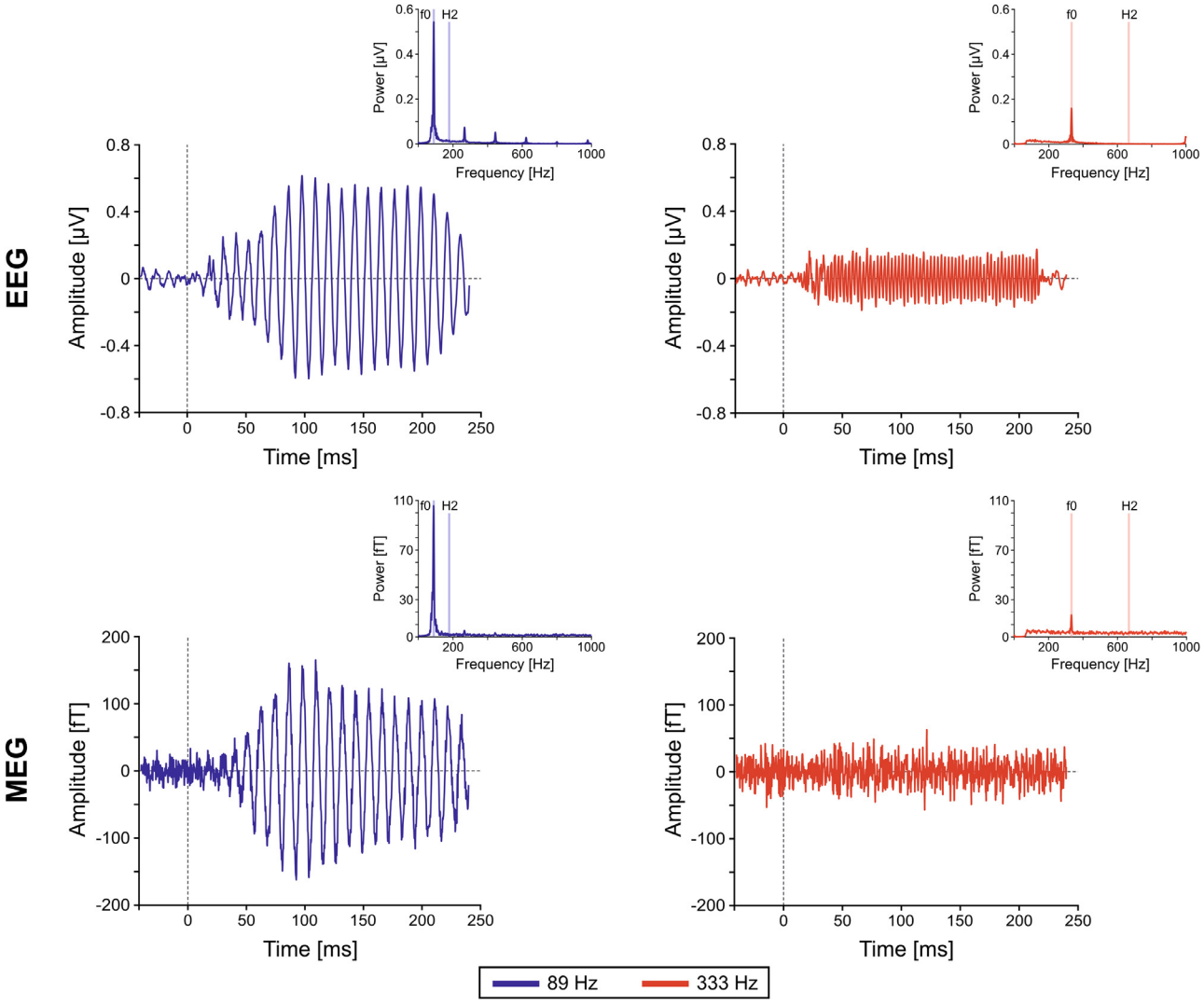

Fig. 1. Grand-averaged time and frequency domain representations of the EEG and MEG FFRs to low and high frequency conditions. Grand-averaged time course and spectral representations of the EEG and MEG recorded FFRs elicited to low (89 Hz; blue) and high (333 Hz; red) frequencies. Both EEG and MEG FFRs represented are a single-channel grand-average across participants ($n = 19$). EEG data displayed was extracted from Cz electrode and MEG data was extracted from a single channel that was most correlated with the EEG channel per subject. Both EEG and MEG data were preprocessed as detailed in the methods subSection 2.4. and grand-averaged across subjects to display the time-domain representation. To obtain the power spectral domain of the different time series, Fast Fourier Transform was applied to zero-padded (1-Hz resolution) averages, windowed with a 5-ms raised cosine ramp. FFRs are observable in the time domain and a clear peak is observed on the fundamental frequency of the stimulus frequency using both recording techniques for the two tested frequencies. f0 = Fundamental Frequency; H2 = Second Harmonic. (For interpretation of the references to colour in this figure legend, the reader is referred to the web version of this article.)

MEG showed clear peaks at the f0 of the stimulus for both frequency conditions; smaller harmonic peaks (integer multiples of the f0) were observable for the low frequency condition only, and with very much attenuated amplitude in the MEG recordings. For the entire analysis and the results presented here, FFRs elicited to the two stimulus polarities were subtracted. Although this method might be controversial when analyzing neural responses to amplitude modulated and speech stimuli (Easwar et al., 2014), adding the FFRs to the two polarities when using pure tones will result in doubling the stimulus frequency due to the half-wave rectification of the signal at the cochlea, whilst the subtraction artificially reconstitutes the stimulus components present in the response and maintains the frequency of the stimulus (Aiken and Picton, 2008; Skoe and Kraus, 2010; Krizman and Kraus, 2019). For the present study, single polarity and averaged polarities grand-average waveforms of FFRs recorded with EEG and MEG and elicited to both frequency conditions are presented for illustration of these phenomena in supplementary Figures 1 and 2 respectively.

3.1. Region of interest analysis from distributed source modeling

To disentangle the contributions of subcortical and cortical FFR sources in both stimulus frequencies, we estimated the neural origin of the FFR using a depth-weighted minimum-norm estimate (wMNE) modeling and extracted the data from bilateral pairs of regions of interest (ROIs) distributed throughout the auditory hierarchy, as well as from two control regions located in the frontal and occipital poles, at maximal distance from the areas of interest. We then compared the signal-to-baseline ratio in each of the auditory ROIs to the signal-to-baseline ratio in the control areas for each frequency presented (Fig. 2).

When analyzing the overall auditory-to-control effects, the FFRs showed a significant effect for Frequency ($F(1,18) = 50.742$, $p < 0.001$, $\eta^2_{partial} = 0.738$; Fig. 3). The overall auditory-to-control ratio was larger in the low frequency condition (mean = 4.404 dB, SE = 0.472 dB) compared to the high frequency condition (mean = 0.843 dB, SE = 0.407 dB), thus indicating that stimulus frequency had a significant effect on the

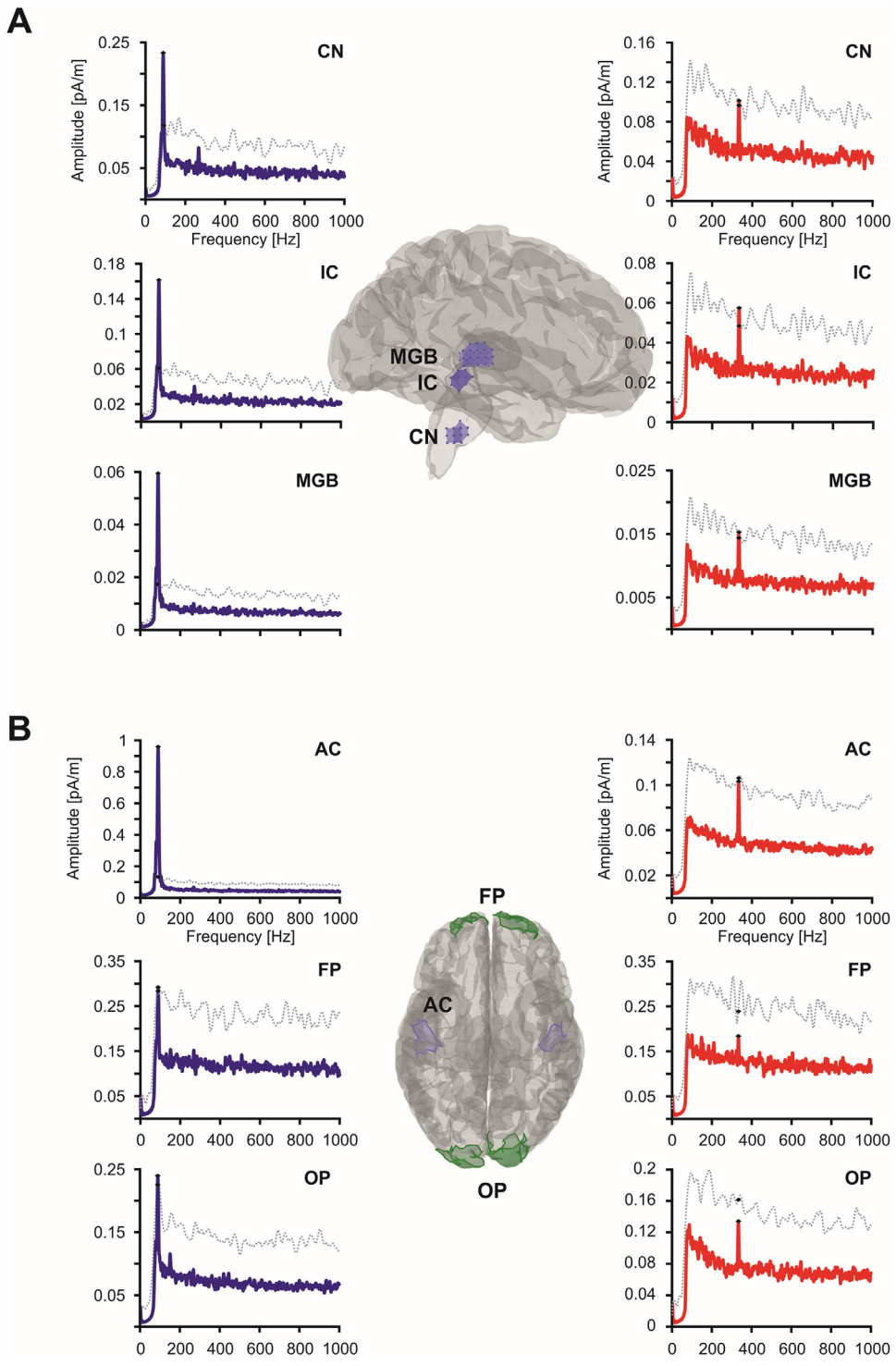

Fig. 2. ROI amplitude spectrogram during FFR and baseline for both frequency conditions. Amplitude spectrograms of the time course extracted from the different regions of interest defined for isolating the neural contributors of the FFR. (A) Subcortical auditory ROIs amplitude spectrogram and (B) Cortical auditory and control ROIs amplitude spectrogram during the FFR (30–210 ms, bold lines) and the baseline (−40–0 ms, dashed lines) time periods for stimulation with low (left column panels; blue) and high (right column panels; red) frequency stimuli. The peaks in the frequency of interest for both FFR and baseline periods are marked with a black diamond. All the results are averaged across bilateral ROIs and across participants. CN, cochlear nucleus; IC, inferior colliculus; MGB, medial geniculate body of the thalamus; AC, auditory cortex; FP, frontal pole; OP, occipital pole. (For interpretation of the references to color in this figure legend, the reader is referred to the web version of this article.)

amplitude of the FFR. ROI effects were also statistically significant ($F(3,54) = 16.872$, $p < 0.001$, $\eta^2_{partial} = 0.484$; Fig. 3), as well as the interaction between Frequency and ROI ($F(3,54) = 36.045$, $p < 0.001$, $\eta^2_{partial} = 0.667$; Fig. 3), providing evidence that the four auditory source generators not only contribute differently to the aggregate FFR response but also have different contribution depending on the frequency of the eliciting stimulus.

To specifically analyze the contribution of each auditory ROI to the FFR for each stimulus frequency separately, we compared the signal-to-baseline ratio in each of the auditory ROIs to the signal-to-baseline ratio in the control areas. For the low frequency condition, the analysis yielded strong peaks at the f0 in all the subcortical auditory ROIs that were significantly larger than the residual signal observed in the control regions (CN: $Z = -3.421$, exact $p < 0.001$; IC: $Z = -3.743$, exact $p < 0.001$; MGB: $Z = -3.783$, exact $p < 0.001$; Fig. 3). A significant peak was also observed for the primary auditory cortex ROI (PAC: $Z = -3.823$, exact $p < 0.001$; Fig. 3), indicating that the neural activity at 89 Hz was larger than the one in the control regions. When applying the windowed FFT analysis on the FFR period the same results were obtained, with strong peaks at the f0 in all the subcortical and the cortical auditory ROIs

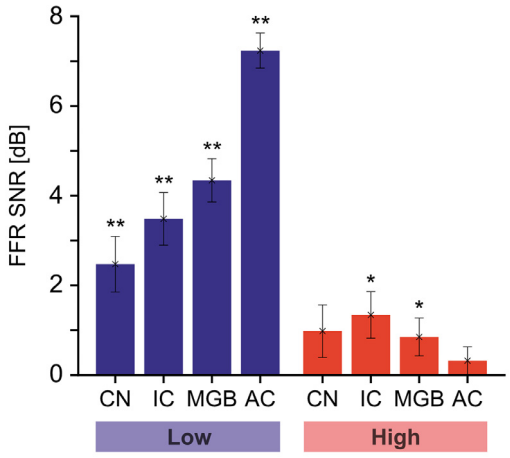

Fig. 3. FFR Auditory-to-control ratio in the different auditory regions of interest for the two frequency conditions. FFR auditory-to-control ratio in each of the different auditory ROIs for the low (blue) and high (red) frequency stimuli. The auditory-to-control ratios depicted in the figure were computed in two steps. First, a signal-to-baseline ratio in each of the auditory and control ROIs was computed, where the signal corresponds to the fundamental frequency mean amplitude, extracted from a 5-Hz window during the FFR period (30 to 210 ms from stimulus onset), and baseline corresponds to the fundamental frequency mean amplitude extracted from the baseline period (−40 to 0 ms from stimulus onset). In a second step, the signal-to-baseline ratio of the control regions was averaged to serve as 'control' in the final auditory-to-control ratio, where the 'auditory' was each of the signal-to-baseline ratios of the different auditory ROIs computed in the first step. Significant auditory-to-control ratios were observed in the four auditory ROIs for the low frequency stimulation, both in subcortical and cortical structures, indicating that all the structures in the auditory pathway under analysis indeed contribute to the aggregate FFR recorded at the scalp. On the other hand, in the high frequency condition, only the IC ROI contributed significantly to the recorded FFR. All the results are averaged across bilateral ROIs and across participants. Error bars represent ± 1 SEM. Statistically significant comparisons are marked with one (p<0.05) or two (p<0.001) asterisks. (For interpretation of the references to color in this figure legend, the reader is referred to the web version of this article.)

compared to the residual signal from the control regions (Supplementary Table 1).

Regarding the results obtained for the high frequency condition, the analysis revealed that only the IC and the MGB ROIs significantly contributed to the recorded FFR (IC: Z = −2.736, exact p = 0.002; MGB: Z = −2.294, exact p = 0.010; Fig. 3). The peak observed at the f0 in the CN ROI showed a tendency towards significance compared to the control regions (Z = −1.569, exact p = 0.062; Fig. 3). Finally, the neural activity recorded from the AC did not show any significant peak at the f0 compared to control regions (AC: Z = −0.805, exact p = 0.221; Fig. 3). Similar results were observed when computing the FFT from the FFR period with 40 ms sliding windows. Both IC and MGB ROIs significantly contributed to the recorded FFR, although only the MGB ROI statistical significance survived correction for multiple comparisons (Supplementary Table 1). The neural activity recorded from the CN showed a tendency towards significance, and the AC ROI did not show any significant peak at f0 compared to the residual activity of the control regions.

3.2. Comparison of the forward projection of the auditory ROIs

The sensor projected source distribution from the MEG recorded FFR, as well as the sensor projected source distribution from each left-right pair of auditory system ROIs for each stimulus frequency, obtained by applying a forward projection through the MEG head model can be observed in Fig. 4A. This analysis allows us to obtain simulated time-domain reconstructions and topographies as if only the selected bilateral auditory ROI was actively contributing to the recorded signal and compare them to the actual sensor projected source distribution from the recorded signal.

As illustrated in the Figure, the subcortical auditory ROIs (CN, IC and MGB) had a similar surface distribution in the low and high frequency conditions. On the other hand, there was an evident rightwards asymmetry in the primary cortex auditory ROI simulation in the low frequency condition, as compared to a bilateral activation in the high frequency condition. The FFR topographies for the MEG recorded data in both frequency conditions revealed a rightwards asymmetry on the low frequency condition, consistent with the asymmetry observed in the simulated data from the primary auditory cortex ROI and with this ROI being main contributor to the recorded FFR response (Fig. 3). This topographical distribution similarity between the recorded FFR topography and the AC ROI topography was confirmed by the Dissimilarity Index analysis (Fig. 4B), which revealed that the AC had a lower index (Dissimilarity Index = 0.3164) and, therefore was the one with a higher similarity with the recorded FFR topography.

On the other hand, the MEG recording topography for the high frequency condition revealed a bilateral activation, reflecting the bilateral activation observed in the subcortical ROI simulation topographies and the IC being the main contributor to the recorded FFR (Fig. 3). This topographical distribution similarity between the recorded FFR topography and the IC ROI topography was confirmed by the Dissimilarity Index analysis (Fig. 4B), which revealed that the IC had a lower index (Dissimilarity Index = 0.3330) and, therefore was the one with a higher similarity with the recorded FFR topography.

3.3. Hemispheric asymmetries of the cortical FFR

To test for the significance of the cortical hemispheric asymmetry observed in the data, we compared f0 amplitude in the right versus left AC ROIs for each frequency condition, using the data from the mixed model described in Fig. 2. In the low frequency condition, the right AC ROI amplitude (mean = 1.230 pA/m, SE = 1.317 pA/m) was significantly stronger than the left AC ROI amplitude (mean = 0.702 pA/m, SE = 0.52 pA/m; Wilcoxon signed-rank test: Z= −3.823, p<0.001; Fig. 5), thus revealing a rightward asymmetry on the low frequency condition in line with the previous results.

On the other hand, in the high frequency condition there was no statistically significant difference between the right (mean = 0.105 pA/m, SE = 0.056 pA/m) and left (mean = 0.102 pA/m, SE = 0.045 pA/m) AC ROIs f0 amplitude (Wilcoxon signed-rank test: Z = −0.201, p = 0.841; Fig. 5), also in line with previously reported results showing that the FFR elicited to the high frequency stimulus had a bilateral topography (results subSection 3.2) and demonstrated that the AC does not contribute significantly to the aggregate FFR response (results subSection 3.1).

4. Discussion

The present study provides a compelling demonstration, using magnetoencephalography, that the FFR reflects the aggregate neural activity in the different stations of the human auditory pathway whose relative contribution varies systematically across the different anatomical levels and in a stimulus (i.e., frequency) dependent manner. In particular, we have observed that whilst the neural contribution of subcortical sources was present for both stimulation frequencies (i.e., low, 89 Hz, and high, 333 Hz), the cortical source was not significantly activated when the eliciting frequency was high. These results favor the multiple generator hypothesis which states that the different nuclei of the human auditory pathway contribute differently to the scalp measured response, and that the specific mixture of sources varies depending on the stimulus characteristics, but they function jointly to provide an accurate processing of periodic sounds (Coffey et al., 2019; Gardi et al., 1979; Tichko and Skoe, 2017).

In particular, our results demonstrate that the neural contributions to the encoding of low frequency sounds is not restricted to subcortical

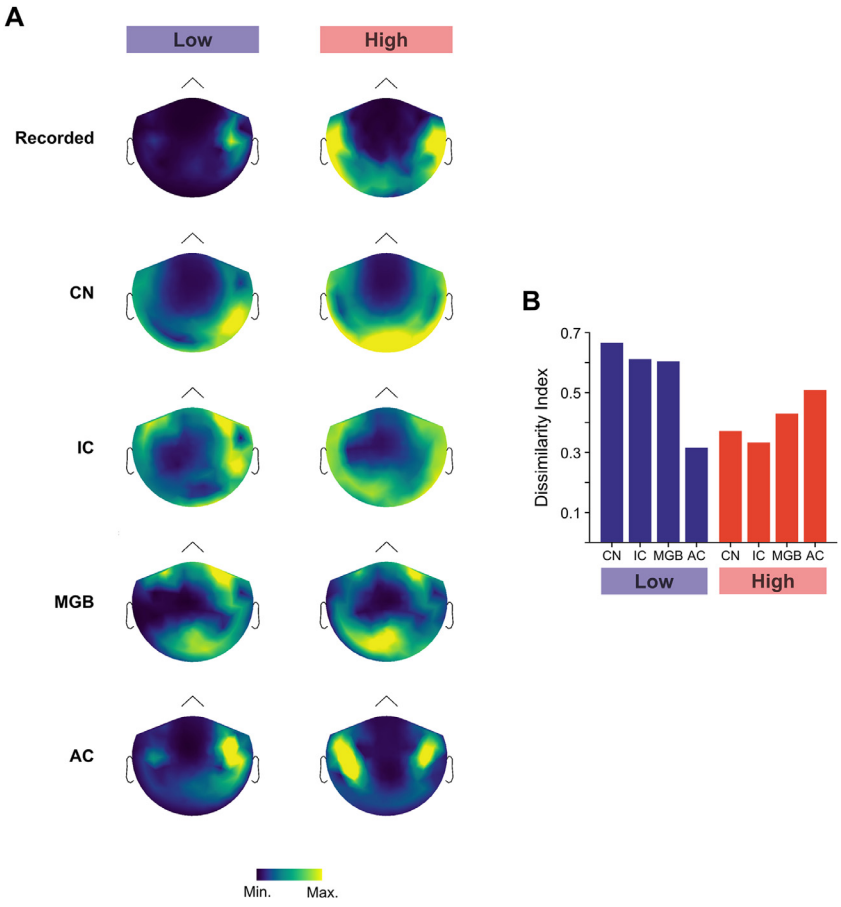

Fig. 4. Sensor-projected source distributions from the MEG recorded data and the different anatomical regions of interest for the two frequency conditions. (A) Sensor distribution topographies from the MEG recorded data and simulated sensor distribution topographies from each left-right pair of auditory system ROIs for the low (89 Hz; Left column panels) and high (333 Hz; Right column panels) frequency stimuli in a two-dimensional sensor space. The topographies are computed by applying the MEG forward model to project the MEG time-domain averages and the source magnitudes back to the sensor space for each paired auditory ROI separately. All topographies are averaged across participants ($n = 19$). The color map is scaled to minimum and maximum signal strength for each ROI to visually depict the sensor distribution to each source. (B) Dissimilarity Index values of the comparison between the sensor-projected topography of the MEG recorded data and each of the auditory regions of interest source distribution topographies for the low and high frequency conditions. The dissimilarity index is a topographical measure of global dissimilarity that can range from 0 (topographic homogeneity) to 2 (topographic inversion). CN, cochlear nucleus; IC, inferior colliculus; MGB, medial geniculate body of the thalamus; AC, auditory cortex. (For interpretation of the references to color in this figure legend, the reader is referred to the web version of this article.)

nuclei as the FFR recorded in the scalp represent an integrated response of different neuronal aggregates throughout the entire auditory hierarchy, including subcortical nuclei and cortical areas. By using distributed source modeling, which allowed us to model and estimate the neural activity of a large number of dipoles based on spatial priors, we showed that the signal-to-noise ratio attributed to the different subcortical and cortical auditory regions was greater than the neural activity from the control regions, located in the frontal and occipital poles. On the other hand, the neural generators of the FFR elicited to high frequency sounds were restricted to subcortical stations only, as the signal-to-noise ratio attributed to cortical auditory regions did not differ from the signal in control regions, thus indicating that no significant cortical contribution was present. These results provide evidence that high frequency sounds-elicited FFRs represent only subcortical activity and, therefore, support the view that the FFR can still be considered, when elicited to sounds of high frequencies, as a window into human subcortical auditory function.

Our findings highlight two of the main axioms recently proposed for the auditory system (Coffey et al., 2019). First, that the central auditory system is a network of structures that are deeply interconnected (Kraus and White-Schwoch, 2015), so that the same auditory structures can engage different neural activation patterns depending on the sound's properties (Krizman and Kraus, 2019; Tichko and Skoe, 2017) and context (Carbajal and Malmierca, 2018; Gorina-Careta et al., 2016; Shiga et al., 2015; Skoe et al., 2014; Slabu et al., 2012). Second, that phase-locking, the phenomenon by which neurons fire at a particular phase within the stimulus cycle and, therefore, synchronize their activity to the incoming stimulus periodic features, is a common functional property throughout the human auditory system. Despite being a common functional property, the phase-locking capabilities of the neuronal aggregates along the different stations of the auditory hierarchy are not identical as it has been demonstrated that the upper limit of temporal precision in phase-locked firing reduces as ascending through the auditory neuraxis (Batra et al., 1989; Joris et al., 2004; Langner, 1992). In other words, our results highlight the fact that both cortical and subcortical structures of the auditory hierarchy are potential generators of the FFR but that the final FFR source configuration to a given stimulus varies with stimulus frequency.

The importance of stimulus frequency for the FFR source configuration is not a novel concept. Previous studies focused on the neural contributors to the FFRs elicited to low stimulus frequencies, and documented that despite the evidence from seminal studies supporting a subcortical origin of the FFR (Gardi et al., 1979; Langner and Schreiner, 1988; Marsh et al., 1970; Smith et al., 1975; Sohmer et al., 1977; Weinberger et al., 1970), cortical areas also contribute to the FFR source configuration (Bidelman, 2018, 2015; Bidelman and Momtaz, 2020; Coffey et al., 2016). In particular, Coffey et al. (2016) reported, using MEG, that for low frequency sounds with a fundamental frequency close to 100 Hz, the AC accounted for the highest relative percentage of signal, followed by contributions from the CN, MGB and IC. On the other hand, Bidelman (2018) analyzed the neural sources of the FFR using EEG and revealed important frequency-specific nuances to Coffey et al. (2016) MEG source interpretation. Specifically, he described that on the low frequency range there was a statistically reliable contribution during the FFR of the auditory nerve, the brainstem and the right AC, agreeing with the MEG study in regards of a putative cortical contribution to the FFR at low frequencies but differing on the dominance of the contributors. Additionally, when analyzing the higher spectral harmonic frequencies in his stimulus, the author observed that in contrast with the low frequency, the primary AC showed no reliable contribution to the FFR, whereas the auditory nerve and the brainstem generators remained robust. In contrast with Coffey et al. (2016) MEG study, Bidelman (2018) reported that the FFR is dominated by subcor-

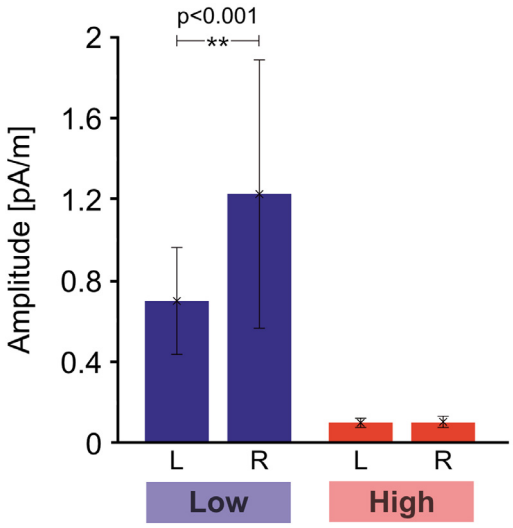

Fig. 5. Hemispheric asymmetry of the cortical FFR for the two frequency conditions. Fundamental frequency amplitude during the FFR period (30 to 310 ms) in the left and right auditory cortex regions of interest for the low (blue) and high (red) frequency stimuli. The fundamental frequency amplitude is extracted from the ROI amplitude spectrograms computed using the mixed surface-volume model in Fig. 2. A significant right-wards asymmetry is observed for the low frequency condition, where there was observed a significant cortical contribution to the recorded FFR. On the other hand, in the high frequency condition, no difference is observed between the left and right auditory cortices contribution. The results are averaged across participants (n = 19). Error bars represent ± 1 SEM. Statistically significant comparisons are marked with two (p<0.001) asterisks. (For interpretation of the references to color in this figure legend, the reader is referred to the web version of this article.)

tical generators and attributed the cortical dominance observed on the MEG study to the natural sensitivity of the MEG recording technique to superficial brain areas. However, all these results cannot be interpreted as indicating a cut-off limit of phase-locking in the cortex and a frequency limit for a cortical contribution to the recorded FFR. Indeed, these previous results are based on the comparison between the neural generators contributing to the encoding of the fundamental frequency or to higher spectral harmonic frequencies and the two measures do not necessarily reflect the same features of speech, besides they show behavioral dissociation (Aiken and Picton, 2008; Kraus and Nicol, 2005) and, therefore, one should be cautious in assuming that both sound features have the same neural sources.

Further studies also proved that the FFR at any given frequency can reflect the activity from multiple generators which phase-lock to the incoming stimulus at different latencies (Holmes et al., 2018; Tichko and Skoe, 2017). Indeed, a computational model supported the idea that whilst both subcortical and cortical generators are activated by low frequency tones, the cortex becomes less sensitive to frequencies higher than 100 Hz (Tichko and Skoe, 2017). This modulation of the FFR source configuration depending on the stimulus frequency is also present when the stimulus frequency is theoretically high enough to reflect neural activity generated exclusively from subcortical structures, both for the fundamental frequency and for higher harmonics of the FFR (Zhang and Gong, 2019).

In the present study we compared the FFR of two pure tones of different frequencies so that we are able to observe how the neural generators of the FFR are modulated by the intrinsic fundamental frequency of the stimulus, thus avoiding the limitations of previous studies (Bidelman, 2018; Bidelman and Momtaz, 2020). Our results favor the importance of frequency for the FFR source configuration to a given stimulus and provide evidence to converge the differential observations regarding the relative contributions of the different auditory neural generators to the FFR obtained with MEG (Coffey et al., 2016) and EEG recordings (Bidelman, 2018; Bidelman and Momtaz, 2020; Zhang and Gong, 2019). Specifically, and in agreement with previous results, we observed a primary cortical contribution to the FFRs elicited to the low frequency stimulation, together with a contribution of the MGB, IC and CN. Regarding the contributors to the high frequency FFRs, our results demonstrate a primary contribution of the IC and the MGB and, despite the bias of the MEG to superficial brain areas (Baillet, 2017; da Silva, 2010), no cortical contribution was observed. Although this hierarchy of contributions to the FFR could be attributed to the natural bias of MEG towards superficial brain generators and the relative contributions of the different auditory areas to the scalp-recorded FFR be weighted differently, it is important to highlight that our results replicate and extend the existing literature and demonstrate that whilst there is indeed a cortical contribution to the low frequency recorded FFR, no cortical contribution is observed as we increase the frequency of the presented stimulus and only the subcortical auditory stations contribute to the scalp-recorded FFR, with a primary contribution coming from the IC and the MGB.

It should be noted however, that MEG and EEG techniques have different sensitivities to the underlying sources and therefore, it should not be assumed that the reported relative weighting of the different neural generators that contribute to the FFR is equal with both recording techniques. This difference can be observed on the topographies of the EEG and MEG recorded FFRs for the two used frequencies in this study. As depicted in the results, the EEG topographies show a main activation of the central regions of the head, whilst on the MEG recorded ones there is an activation on the primary auditory cortices, thus demonstrating the natural sensitivity of the MEG to superficial brain areas but also the more accurate source localization sensitivity of it due to the lack of spread through the head of the magnetic signals (Baillet, 2017; da Silva, 2010). Nevertheless, and despite the sensitivities of the different techniques, the different underlying neural generators of the FFR depending on the frequency is also reflected in the overall power difference between the low and the high frequency recorded FFRs in both the MEG and EEG recordings. In particular, the low frequency FFRs have an enhanced amplitude compared to the high frequency FFRs, difference that can be attributed to the fact that for the low frequency condition the FFR source configuration has a cortical component which is closer to the scalp and, therefore, both recording techniques are more sensitive to the aggregate generated signal.

In addition to the difference in amplitude between low and high frequency conditions, the MEG topographies obtained for the low frequency showed an asymmetry towards the right auditory cortex. This asymmetry is also depicted on the forward projections of each bilateral pair of ROIs (Fig. 4), which represent how the information modelled as originating in the different auditory ROIs would be distributed over sensors taking into account the orientation of the sources. The topographic distribution of the forward projections was very similar for the significant subcortical ROIs contributing to the FFR source configuration for each frequency condition. Additionally, an evident asymmetry was observed on the AC ROI of the low frequency condition. This rightwards asymmetry replicates previous findings (Coffey et al., 2017, 2016) and would serve to support the observed relationship of FFR with behavior (Bianchi et al., 2017; Coffey et al., 2016; Zhang and Gong, 2019) and its modulation with attention (Hartmann and Weisz, 2019; Holmes et al., 2018). Interestingly, this asymmetry observed on the MEG topographies for the low frequency but not for the high frequency condition complement the findings of a recent study that took a more direct approach to disentangle the underlying generators of the FFR by, instead of reconstructing the sources from the scalp recorded signal, recording the FFR before and after a transient inactivation of the right primary AC by means of the repetitive transcranial magnetic stimulation (rTMS)-patterned protocol known as the continuous theta burst stimulation (cTBS) (López-Caballero et al., 2020). In their study, stimuli of two different frequencies were also used (113 and 317 Hz), while no effects of

cTBS were observed in either FFR or cortical potentials, which lead the authors to argue that the inactivation of an auditory sensory area with this protocol was ineffective or maybe compensated by the left auditory cortex after the transient inactivation of the right one. Our results complement their findings by showing that, for the low frequency condition, the inactivation of the right auditory cortex was pointing on the right direction, but despite the right asymmetry, a contribution from the left auditory cortex was still observable (Fig. 5), which could compensate for the inactivation of the right one. Regarding their results for the high frequency condition, we showed that no cortical contribution could be observed when the FFR was elicited to high frequency stimuli, which could have been the reason why their inactivation of the primary auditory cortex had no effect on the scalp-recorded FFR.

A limitation of the present study is that, when applying a sliding window analysis on the FFT to compensate for the different length of the baseline and FFR periods, the contribution of the IC to the high frequency FFRs did not survive correction for multiple comparisons. This result does not invalidate the main contribution of the present study, as the subcortical contribution to the high frequency stimuli was confirmed by the contribution of the MGB to the scalp recorded FFR, which did survive the correction for multiple comparisons, as by the contribution of the IC, which was also significant per se. Taking into account that the MEG signal recorded on the high frequency condition had a reduced amplitude in comparison with the low frequency condition (see corresponding spectra in Fig. 1), by computing the FFT with a shorter time window the amount of signal is hence reduced, resulting in a lack of statistical power. In comparison, the analysis with a longer FFT window on the FFR period provides enough points of data for the results to survive the multiple comparisons correction. This is an important aspect to consider in future FFR studies, so that the recorded baseline period is long enough to allow applying a time window of similar length as for FFR period, so that enough data is available for reaching appropriate statistical power.

Summing up, our results confirm and extend the previous literature and demonstrate that whilst for sounds with a fundamental frequency circa 100 Hz, at the limit of phase-locking capabilities of cortical neurons, there is an evident contribution from the auditory cortex to the FFR source configuration, FFRs for high frequency sounds originate from subcortical auditory stations with no cortical contribution at all. Therefore, not only FFR source configurations are variable depending on the frequency but also the engagement of some of the expected neural contributors (i.e., the engagement of the auditory cortex) is frequency-dependent.

We extend previous studies by demonstrating that not only the encoding of higher spectral harmonics of a low frequency sound have only subcortical neural contributors but also the encoding of sounds with high frequency f0. This leads us to hypothesize that it could be possible that despite the fact that the fundamental frequency and the formants show a behavioral dissociation, they both rely on the subcortical encoding of the incoming sounds as an anchor for further processing. This hypothesis would apply also to previous results reporting that subcortical synchrony is necessary to generate a scalp-recorded FFR (White-Schwoch et al., 2019) and training-dependent changes in pitch processing arise a subcortical level (Bianchi et al., 2017), together with evidence that subcortical auditory synchrony deficits may constitute a pre-reading risk factor in the emergence of dyslexia (De Vos et al., 2020).

The hypothesized subcortical anchoring, together with what we observed in the present study, take us to hypothesize that subcortical synchrony is key for sound encoding and provides the basis for further sensory sound processing that takes place along the entire auditory hierarchy. In this synchrony in the subcortical auditory nuclei provides an anchor to the voice of the speaker in an everyday situation and deficits on the synchronization could produce consequences on basic sound processing, language acquisition or language and auditory disorders.

Declaration of Competing Interest

The authors declare no competing financial interests.

Acknowledgments

This work was supported by the PSI2015-63664-P project (MINECO/FEDER) and the ICREA Academia Distinguished Professorship awarded to Carles Escera, by the María de Maeztu Unit of Excellence (Institute of Neurosciences, University of Barcelona) MDM-2017-0729, Ministry of Science, Innovation and Universities, and the Academy of Finland (Project No. 273134 for P.A.). We would like to thank Dr. Jordi Costa-Faidella for his support on the analysis and Iiris Kyläheiko and Pyry Heikkinen for help in data collection.

Data and Code Availability Statement

Pre-processed MEG and EEG data will be available on request to the corresponding author. All custom-written code used is also available upon request to the corresponding author.

Supplementary materials

Supplementary material associated with this article can be found, in the online version, at doi:10.1016/j.neuroimage.2021.117866.

References

Aiken, S.J., Picton, T.W., 2008. Envelope and spectral frequency-following responses to vowel sounds. Hear. Res. 245, 35–47. doi:10.1016/j.heares.2008.08.004.

Anderson, S., 2017. Clinical translation: aging, hearing loss, and amplification. In: Kraus, N., Anderson, S., White-Schwoch, T., Fay, R.R., Popper, A.N. (Eds.), The Frequency-Following Response. Springer Handbook of Auditory Research, 61. Springer, Cham, pp. 267–294. doi:10.1007/978-3-319-47944-6_11.

Anderson, S., Skoe, E., Chandrasekaran, B., Kraus, N., 2010. Neural timing is linked to speech perception in noise. J. Neurosci. 30, 4922–4926. doi:10.1523/JNEUROSCI.0107-10.2010.

Attal, Y., Schwartz, D., 2013. Assessment of subcortical source localization using deep brain activity imaging model with minimum norm operators: a MEG study. PLoS ONE 8. doi:10.1371/journal.pone.0059856.

Baillet, S., 2017. Magnetoencephalography for brain electrophysiology and imaging. Nat. Neurosci. 20, 327–339. doi:10.1038/nn.4504.

Banai, K., Ahissar, M., 2006. Auditory processing deficits in dyslexia: task or stimulus related? Cereb. Cortex 16, 1718–1728. doi:10.1093/cercor/bhj107.

Banai, K., Hornickel, J., Skoe, E., Nicol, T., Zecker, S., Kraus, N., 2009. Reading and subcortical auditory function. Cereb. Cortex 19, 2699–2707. doi:10.1093/cercor/bhp024.

Banai, K., Nicol, T., Zecker, S.G., Kraus, N., 2005. Brainstem timing: implications for cortical processing and literacy. J. Neurosci. 25, 9850–9857. doi:10.1523/JNEUROSCI.2373-05.2005.

Batra, R., Kuwada, S., Stanford, T.R., 1989. Temporal coding of envelopes and their interaural delays in the inferior colliculus of the unanesthetized rabbit. J. Neurophysiol. 61, 257–268.

Bianchi, F., Hjortkjær, J., Santurette, S., Zatorre, R.J., Siebner, H.R., Dau, T., 2017. Subcortical and cortical correlates of pitch discrimination: evidence for two levels of neuroplasticity in musicians. Neuroimage 163, 398–412. doi:10.1016/j.neuroimage.2017.07.057.

Bidelman, G.M., 2018. Subcortical sources dominate the neuroelectric auditory frequency-following response to speech. Neuroimage 175, 56–69. doi:10.1016/j.neuroimage.2018.03.060.

Bidelman, G.M., 2015. Multichannel recordings of the human brainstem frequency-following response: scalp topography, source generators, and distinctions from the transient ABR. Hear. Res. 1–13. doi:10.1016/j.heares.2015.01.011.

Bidelman, G.M., Krishnan, A., Gandour, J.T., 2011. Enhanced brainstem encoding predicts musicians' perceptual advantages with pitch. Eur. J. Neurosci. 33, 530–538. doi:10.1111/j.1460-9568.2010.07527.x.

Bidelman, G.M., Momtaz, S., 2020. Subcortical sources drive the relation between frequency-following responses (FFRs) and speech-in-noise perception. bioRxiv doi:10.1101/2020.03.29.014233.

Carbajal, G.V., Malmierca, M.S., 2018. The neuronal basis of predictive coding along the auditory pathway: from the subcortical roots to cortical deviance detection. Trends Hear. 22, 233121651878482. doi:10.1177/2331216518784822.

Carcagno, S., Plack, C.J., 2017. Short-Term Learning and Memory: training and Perceptual Learning. In: Kraus, N., Anderson, S., White-Schwoch, T., Fay, R.R., Popper, A.N. (Eds.), The Frequency-Following Response. Springer Handbook of Auditory Research, 61. Springer, Cham, pp. 75–100. doi:10.1007/978-3-319-47944-6_4.

Carcagno, S., Plack, C.J., 2011. Subcortical plasticity following perceptual learning in a pitch discrimination task. JARO - J. Assoc. Res. Otolaryngol. 12, 89–100. doi:10.1007/s10162-010-0236-1.

Chandrasekaran, B., Hornickel, J., Skoe, E., Nicol, T., Kraus, N., 2009. Context-dependent encoding in the human auditory brainstem relates to hearing speech in noise: implications for developmental dyslexia. Neuron 64, 311–319. doi:10.1016/j.neuron.2009.10.006.

Chandrasekaran, B., Kraus, N., 2010. The scalp-recorded brainstem response to speech: neural origins and plasticity. Psychophysiology 47, 236–246. doi:10.1111/j.1469-8986.2009.00928.x.

Chandrasekaran, B., Skoe, E., Kraus, N., 2014. An integrative model of subcortical auditory plasticity. Brain Topogr 27, 539–552. doi:10.1007/s10548-013-0323-9.

Coffey, E.B.J., Herholz, S.C., Chepesiuk, A.M.P., Baillet, S., Zatorre, R.J., 2016. Cortical contributions to the auditory frequency-following response revealed by MEG. Nat. Commun. 7, 11070. doi:10.1038/ncomms11070.

Coffey, E.B.J., Musacchia, G., Zatorre, R.J., 2017. Cortical correlates of the auditory frequency-following and onset responses: EEG and fMRI evidence. J. Neurosci. 37, 830–838. doi:10.1523/JNEUROSCI.1265-16.2017.

Coffey, E.B.J., Nicol, T., White-Schwoch, T., Chandrasekaran, B., Krizman, J., Skoe, E., Zatorre, R.J., Kraus, N., 2019. Evolving perspectives on the sources of the frequency-following response. Nat. Commun. 10, 1–10. doi:10.1038/s41467-019-13003-w.

Cooley, J.W., Tukey, J.W., 1964. An algorithm for the machine calculation complex fourier series. Int. J. Comput. Math. 19, 297–301.

Costa-Faidella, J., Baldeweg, T., Grimm, S., Escera, C., 2011. Interactions between "what" and "when" in the auditory system: temporal predictability enhances repetition suppression. J. Neurosci. 31, 18590–18597. doi:10.1523/JNEUROSCI.2599-11.2011.

Cunningham, J., Nicol, T., Zecker, S.G., Bradlow, A.R., Kraus, N., 2001. Neurobiologic responses to speech in noise in children with learning problems : deficits and strategies for improvement. Clin. Neurophysiol. 112, 758–767.

da Silva, F.H.L., Hansen, P., Kringelbach, M., 2010. Electrophysiological basis of MEG signals. In: Salmelin, R. (Ed.), MEG: An Introduction to Methods. Oxford University Press, New York, NY, US, pp. 1–23. doi:10.1093/acprof:oso/9780195307238.003.0001.

De Vos, A., Vanvooren, S., Ghesquière, P., Wouters, J., 2020. Subcortical auditory neural synchronization is deficient in pre-reading children who develop dyslexia. Dev. Sci. 1–16. doi:10.1111/desc.12945.

Destrieux, C., Fischl, B., Dale, A., Halgren, E., 2010. Automatic parcellation of human cortical gyri and sulci using standard anatomical nomenclature. Neuroimage 53, 1–15. doi:10.1016/j.neuroimage.2010.06.010.

Escera, C., 2017. The role of the auditory brainstem in regularity encoding and deviance detection. In: Kraus, N., Anderson, S., White-Schwoch, T., Fay, R.R., Popper, A.N. (Eds.), The Frequency-Following Response. Springer Handbook of Auditory Research, 61. Springer, Cham, pp. 101–120. doi:10.1007/978-3-319-47944-6_5.

Fischl, B., 2012. FreeSurfer. Neuroimage 62, 774–781. doi:10.1016/j.neuroimage.2012.01.021.

Galbraith, G.C., Threadgill, M.R., Hemsley, J., Salour, K., Songdej, N., Ton, J., Cheung, L., 2000. Putative measure of peripheral and brainstem frequency-following in humans. Neurosci. Lett. 292, 123–127.

Gardi, J., Merzenich, M., Mckean, C., 1979. Origins of the scalp-recorded frequency-following response in the cat. Int. J. Audiol. 18, 353–380. doi:10.3109/00206097909070062.

Gorina-Careta, N., Zarnowiec, K., Costa-Faidella, J., Escera, C., 2016. Timing predictability enhances regularity encoding in the human subcortical auditory pathway. Sci. Rep. 6, 37405. doi:10.1038/srep37405.

Gross, J., Baillet, S., Barnes, G.R., Henson, R.N., Hillebrand, A., Jensen, O., Jerbi, K., Litvak, V., Maess, B., Oostenveld, R., Parkkonen, L., Taylor, J.R., van Wassenhove, V., Wibral, M., Schoffelen, J.M., 2013. Good practice for conducting and reporting MEG research. Neuroimage 65, 349–363. doi:10.1016/j.neuroimage.2012.10.001.

Hämäläinen, M., 2009. MNE Software User's Guide v2.7. MGH/HMS/MIT Athinoula A. (Martinos Cent. Biomed. Imaging) doi:10.1111/j.1462-5822.2009.01352.x.

Hämäläinen, M.S., Lin, F.-H., Mosher, J.C., 2010. Anatomically and functionally constrained minimum-norm estimates. In: Hansen, P., Kringelbach, M., Salmelin, R. (Eds.), MEG: An Introduction to Methods. Oxford University Press, New York, NY, pp. 186–215. doi:10.1093/acprof:oso/9780195307238.003.0008.

Hartmann, T., Weisz, N., 2019. Auditory cortical generators of the Frequency Following Response are modulated by intermodal attention. Neuroimage 203, 116185. doi:10.1016/j.neuroimage.2019.116185.

Hofmeier, B., Wolpert, S., Aldamer, E.S., Walter, M., Thiericke, J., Braun, C., Zelle, D., Rüttiger, L., Klose, U., Knipper, M., 2018. Reduced sound-evoked and resting-state BOLD fMRI connectivity in tinnitus. NeuroImage Clin 20, 637–649. doi:10.1016/j.nicl.2018.08.029.

Holmes, E., Purcell, D.W., Carlyon, R.P., Gockel, H.E., Johnsrude, I.S., 2018. Attentional modulation of envelope-following responses at lower (93–109Hz) but not higher (217–233Hz) modulation rates. J. Assoc. Res. Otolaryngol. Assoc. Res. Otolaryngol. 19, 83–97. doi:10.1007/s10162-017-0641-9.

Hornickel, J., Anderson, S., Skoe, E., Yi, H.G., Kraus, N., 2012. Subcortical representation of speech fine structure relates to reading ability. Neuroreport 23, 6–9. doi:10.1097/WNR.0b013e32834d2ffd.

Hornickel, J., Kraus, N., 2013. Unstable representation of sound: a biological marker of dyslexia. J. Neurosci. 33, 3500–3504. doi:10.1523/JNEUROSCI.4205-12.2013.

Huang, M.X., Mosher, J.C., Leahy, R.M., 1999. A sensor-weighted overlapping-sphere head model and exhaustive head model comparison for MEG. Phys. Med. Biol. 44, 423–440. doi:10.1088/0031-9155/44/2/010.

Jackson, A.F., Bolger, D.J., 2014. The neurophysiological bases of EEG and EEG measurement: a review for the rest of us. Psychophysiology 51, 1061–1071. doi:10.1111/psyp.12283.

Jensen, O., Hesse, C., 2010. Estimating distributed representations of evoked responses and oscillatory brain activity. In: Hansen, P., Kringelbach, M., Salmelin, R. (Eds.), MEG: An Introduction to Methods. Oxford University Press, New York, NY, pp. 156–185. doi:10.1093/acprof:oso/9780195307238.003.0007.

Joris, P.X., Schreiner, C.E., Rees, A., 2004. Neural processing of amplitude-modulated sounds. Physiol. Rev. 84, 541–577. doi:10.1152/physrev.00029.2003.

Kiren, T., Aoyagi, M., Furuse, H., Koike, Y., 1994. An Experimental Study on the Generator of Amplitude-modulation Following Response. Acta Otolaryngol 114, 28–33. doi:10.3109/00016489409128297.

Kraus, N., Anderson, S., White-Schwoch, T., 2017. The Frequency-Following Response: A Window into Human communication, Springer Handbook of Auditory Research. Springer International Publishing, Cham, Switzerland doi:10.1007/978-3-319-47944-6.

Kraus, N., Nicol, T., 2005. Brainstem origins for cortical "what" and "where" pathways in the auditory system. Trends Neurosci 28, 176–181. doi:10.1016/j.tins.2005.02.003.

Kraus, N., Slater, J., 2016. Beyond words: how humans communicate through sound. Annu. Rev. Psychol. 67, 83–103. doi:10.1146/annurev-psych-122414-033318.

Kraus, N., White-Schwoch, T., 2015. Unraveling the biology of auditory learning: a cognitive–sensorimotor–reward framework. Trends Cogn. Sci. 19, 642–654. doi:10.1016/j.tics.2015.08.017.

Krishnan, A., Swaminathan, J., Gandour, J.T., 2008. Experience-dependent enhancement of linguistic pitch representation in the brainstem is not specific to a speech context. J. Cogn. Neurosci. 21, 1092–1105.

Krizman, J., Kraus, N., 2019. Analyzing the FFR: a tutorial for decoding the richness of auditory function. Hear. Res. 382, 107779. doi:10.1016/j.heares.2019.107779.

Krizman, J., Marian, V., Shook, A., Skoe, E., Kraus, N., 2012. Subcortical encoding of sound is enhanced in bilinguals and relates to executive function advantages. Proc. Natl. Acad. Sci. 109, 7877–7881. doi:10.1073/pnas.1201575109.

Krizman, J., Skoe, E., Marian, V., Kraus, N., 2014. Bilingualism increases neural response consistency and attentional control: evidence for sensory and cognitive coupling. Brain Lang 128, 34–40. doi:10.1016/j.bandl.2013.11.006.

Krizman, J., Slater, J., Skoe, E., Marian, V., Kraus, N., 2015. Neural processing of speech in children is influenced by extent of bilingual experience. Neurosci. Lett. 585, 48–53. doi:10.1016/j.neulet.2014.11.011.

Langner, G., 1992. Periodicity coding in the auditory system. Hear. Res. 60, 115–142. doi:10.1016/0378-5955(92)90015-F.

Langner, G., Schreiner, C.E., 1988. Periodicity coding in the inferior colliculus of the cat. I. Neuronal Mechanisms. J. Neurophysiol. 60, 1799–1822. doi:10.1152/jn.1988.60.6.1823.

Li, X., Jeng, F.-.C., 2011. Noise tolerance in human frequency-following responses to voice pitch. J. Acoust. Soc. Am. 129, EL21–EL26. doi:10.1121/1.3528775.

Lin, F.H., Witzel, T., Ahlfors, S.P., Stufflebeam, S.M., Belliveau, J.W., Hämäläinen, M.S., 2006. Assessing and improving the spatial accuracy in MEG source localization by depth-weighted minimum-norm estimates. Neuroimage 31, 160–171. doi:10.1016/j.neuroimage.2005.11.054.

López-Caballero, F., Martin-Trias, P., Ribas-Prats, T., Gorina-Careta, N., Bartrés-Faz, D., Escera, C., 2020. Effects of cTBS on the frequency-following response and other auditory evoked potentials. Front. Hum. Neurosci. 14, 250. doi:10.3389/fnhum.2020.00250.

Marsh, J.T., Worden, F.G., Smith, J.C., 1970. Auditory frequency-following response: neural or artifact? Science 169, 1222–1223.

Moushegian, G., Rupert, A.L., Stillman, R.D., 1973. Scalp-recorded early responses in man to frquencies in the speech range. Electroencephalogr. Clin. Neurophysiol. 35, 665–667.

Mühlau, M., Rauschecker, J.P., Oestreicher, E., Gaser, C., Röttinger, M., Wohlschläger, A.M., Simon, F., Etgen, T., Conrad, B., Sander, D., 2006. Structural brain changes in tinnitus. Cereb. Cortex 16, 1283–1288. doi:10.1093/cercor/bhj070.

Murray, M.M., Brunet, D., Michel, C.M., 2008. Topographic ERP analyses: a step-by-step tutorial review. Brain Topogr 20, 249–264. doi:10.1007/s10548-008-0054-5.

Musacchia, G., Sams, M., Skoe, E., Kraus, N., 2007. Musicians have enhanced subcortical auditory and audiovisual processing of speech and music. Proc. Natl. Acad. Sci. 104, 15894–15898.

Parbery-Clark, A., Skoe, E., Kraus, N., 2009. Musical experience limits the degradative effects of background noise on the neural processing of sound. J. Neurosci. 29, 14100–14107. doi:10.1523/JNEUROSCI.3256-09.2009.

Parbery-Clark, A., Strait, D.L., Kraus, N., 2011. Context-dependent encoding in the auditory brainstem subserves enhanced speech-in-noise perception in musicians. Neuropsychologia 49, 3338–3345. doi:10.1016/j.neuropsychologia.2011.08.007.

Picton, T.W., 2011. Human Auditory Evoked Potentials. Plural Publishing, Inc., San Diego.

Ribas-Prats, T., Almeida, L., Costa-Faidella, J., Plana, M., Corral, M.J., Gómez-Roig, M.D., Escera, C., 2019. The frequency-following response (FFR) to speech stimuli: a normative dataset in healthy newborns. Hear. Res. 371, 28–39. doi:10.1016/j.heares.2018.11.001.

Russo, N., Nicol, T., Musacchia, G., Kraus, N., 2004. Brainstem responses to speech syllables. Clin. Neurophysiol. 115, 2021–2030. doi:10.1016/j.clinph.2004.04.003.

Russo, N., Nicol, T., Trommer, B., Zecker, S., Kraus, N., 2009. Brainstem transcription of speech is disrupted in children with autism spectrum disorders. Dev. Sci. 12, 557–567. doi:10.1111/j.1467-7687.2008.00790.x.

Russo, N., Nicol, T., Zecker, S.G., Hayes, E.a., Kraus, N., 2005. Auditory training improves neural timing in the human brainstem. Behav. Brain Res. 156, 95–103. doi:10.1016/j.bbr.2004.05.012.

Russo, N., Skoe, E., Trommer, B., Nicol, T., Zecker, S.G., Bradlow, A.R., Kraus, N., 2008. Deficient brainstem encoding of pitch in children with Autism Spectrum Disorders. Clin. Neurophysiol. 119, 1720–1731. doi:10.1016/j.clinph.2008.01.108.

Shiga, T., Althen, H., Cornella, M., Zarnowiec, K., Yabe, H., Escera, C., 2015. Deviance-related responses along the auditory hierarchy: combined FFR, MLR and MMN evidence. PLoS ONE 10, 1–14. doi:10.1371/journal.pone.0136794.

Skoe, E., Burakiewicz, E., Figueiredo, M., Hardin, M., 2017. Basic neural processing of sound in adults is influenced by bilingual experience. Neuroscience 349, 278–290. doi:10.1016/j.neuroscience.2017.02.049.

Skoe, E., Chandrasekaran, B., Spitzer, E.R., Wong, P.C.M., Kraus, N., 2014. Human brainstem plasticity: the interaction of stimulus probability and auditory learning. Neurobiol. Learn. Mem. 109, 82–93. doi:10.1016/j.nlm.2013.11.011.

Skoe, E., Kraus, N., 2012. A little goes a long way: how the adult brain is shaped by musical training in childhood. J. Neurosci. 32, 11507–11510. doi:10.1523/JNEUROSCI.1949-12.2012.

Skoe, E., Kraus, N., 2010a. Auditory brain stem response to complex sounds: a tutorial. Ear Hear 31, 302–324. doi:10.1097/AUD.0b013e3181cdb272.

Skoe, E., Kraus, N., 2010b. Hearing it again and again: on-line subcortical plasticity in humans. PLoS ONE 5, 1–9. doi:10.1371/journal.pone.0013645.

Skoe, E., Krizman, J., Spitzer, E., Kraus, N., 2015. Prior experience biases subcortical sensitivity to sound patterns. J. Cogn. Neurosci. 27, 124–140. doi:10.1162/jocn_a_00691.

Skoe, E., Krizman, J., Spitzer, E.R., Kraus, N., 2013. The auditory brainstem is a barometer of rapid auditory learning. Neuroscience 243, 104–114. doi:10.1016/j.neuroscience.2013.03.009.

Slabu, L., Grimm, S., Escera, C., 2012. Novelty detection in the human auditory brainstem. J. Neurosci. 32, 1447–1452. doi:10.1523/JNEUROSCI.2557-11.2012.

Smith, J.C., Marsh, J.T., Brown, W.S., 1975. Far-field recorded frequency-following responses: evidence for the locus of brainstem sources. Electroencephalogr. Clin. Neurophysiol. 39, 465–472.

Sohmer, H., Pratt, H., Kinarti, R., 1977. Sources of frequency following responses (FFR) in man. Electroencephalogr. Clin. Neurophysiol. 42, 656–664. doi:10.1016/0013-4694(77)90282-6.

Song, J., Skoe, E., Banai, K., Kraus, N., 2012. Training to improve hearing speech in noise: biological mechanisms. Cereb. Cortex 22, 1180–1190. doi:10.1093/cercor/bhr196.

Song, J., Skoe, E., Banai, K., Kraus, N., 2011. Perception of speech in noise: neural correlates. J. Cogn. Neurosci. 23, 2268–2279. doi:10.1162/jocn.2010.21556.

Song, J.H., Skoe, E., Wong, P.C.M., Kraus, N., 2008. Plasticity in the adult human auditory brainstem following short-term linguistic training. J. Cogn. Neurosci. 20, 1892–1902. doi:10.1162/jocn.2008.20131.

Tadel, F., Baillet, S., Mosher, J.C., Pantazis, D., Leahy, R.M., 2011. Brainstorm: a user-friendly application for MEG/EEG analysis. Comput. Intell. Neurosci. 2011. doi:10.1155/2011/879716.

Taulu, S., Kajola, M., Simola, J., 2004. Suppression of interference and artifacts by the signal space separation method. Brain Topogr 16, 269–275. doi:10.1023/B:BRAT.0000032864.93890.f9.

Tesche, C.D., Uusitalo, M.A., Ilmoniemi, R.J., Huotilainen, M., Kajola, M., Salonen, O., 1995. Signal-space projections of MEG data characterize both distributed and well-localized neuronal sources. Electroencephalogr. Clin. Neurophysiol. 95, 189–200. doi:10.1016/0013-4694(95)00064-6.

Tichko, P., Skoe, E., 2017. Frequency-dependent fine structure in the frequency-following response: the byproduct of multiple generators. Hear. Res. 348, 1–15. doi:10.1016/j.heares.2017.01.014.

Weinberger, N.M., Kitzes, L.M., Goodman, D.A., 1970. Some characteristics of the “auditory neurophonic. Experientia 26, 46–48. doi:10.1007/BF01900383.

White-Schwoch, T., Anderson, S., Krizman, J., Nicol, T., Kraus, N., 2019. Case studies in neuroscience: subcortical origins of the frequency-following response. J. Neurophysiol. 122, 844–848. doi:10.1152/jn.00112.2019.

Wong, P.C.M., Skoe, E., Russo, N., Dees, T., Kraus, N., 2007. Musical experience shapes human brainstem encoding of linguistic pitch patterns. Nat. Neurosci. 10, 420–422. doi:10.1038/nn1872.

Zhang, X., Gong, Q., 2019. Frequency-following responses to complex tones at different frequencies reflect different source configurations. Front. Neurosci. 13, 1–18. doi:10.3389/fnins.2019.00130.

Zhang, X., Gong, Q., 2017. Correlation between the frequency difference limen and an index based on principal component analysis of the frequency-following response of normal hearing listeners. Hear. Res. 344, 255–264. doi:10.1016/j.heares.2016.12.004.